Proceedings of the 2006 IASME/WSEAS International Conference on Energy & Environmental Systems, Chalkida, Greece, May 8-10, 2006 (pp218-226)

SINGLE PHASE BRUSHLESS DC MOTOR WITH PWM CONTROL STRATEGY AND SPECIAL FORM OF PM ROTOR

SAMEER KHADER
College of Engineering and Technology
Palestine Polytechnic University
Hebron- West Bank
P.O.Box 198, +970 22230068
PALESTINE

ABSTRACT : - This paper describes a mathematical model for electromagnetic simulation of single phase brushless DC motor with special form rotor magnets, stator periphery and stator distributed winding . The rotor permanent magnets are mounted on the rotor in such a way in order to enhance the flux distribution in the airgap so as to reduce the torque fluctuations and achieve the optimized torque. The obtained results are analyzed and decomposed in harmonic spectrum by means of Fast Fourier Transform (FFT) in order to determine the highest order harmonics and the best way to eliminate them. Analytically obtained motor characteristics are discussed for a wide range of parameters such as Pulse Width Modulation (PWM) control strategy, modulation index, induced voltage waveforms and control signal width and shape.

Keywords: DC Motors, Synchronous Motors, and PWM

1. Introduction

Permanent-magnet excited brushless DC motors are becoming increasingly attractive in large number for applications due to performance advantages such as reduced size and cost, reduced torque ripples, increased torque-current ratio, low noises, high efficiency, reduced maintenance and good control characteristics over a wide range in torque–speed plan .

In general Brushless DC motors such as fans are smaller in size and weight than AC fans using shaded pole or Universal motors. Also these motors have an ability to work with the available low voltage sources such as 24-V or 12-V DC supply makes the brushless dc motor fans convenient for use in electronic equipment, computers, mobile equipment, vehicles, and spindle drives for disk memory, because of its high reliability, efficiency, and ability to reverse rapidly. Brushless dc motors in the fractional horsepower range have been used in various types of actuators in advanced aircraft and satellite systems[1-3].

Most popular brushless dc motors are mainly three phases [4-6] which are controlled and driven by full bridge transistor circuits .

Together with applying permanent magnet excitation, it is necessary to obtain an additional torque components. These components can be obtained due to a difference in magnetic permance in both quarter and direct axis, therefore, reluctance torque is developed and torque-null regions are reduced significantly [7,8].

In this paper, a brushless DC motor with distributed winding and special form of PM- rotor with special stator periphery are described. The applied driving circuit consists of four power transistors so as to produce four quadrant operation. The principle of operation of this motor can be explained as follow:

When the transistor is switched on, the current will flow in the armature winding causing magnetic flux which interacts with rotor PM flux. As a result, an electromagnetic torque will be produced causing rotor rotation. At the same time two additional torques are obtained, the first one is called reluctance torque due to difference in the airgap permance, and the other is obtained due to interaction between the stator core and the PM–rotor by means of magnetic reflecting theory" magnetic mirrors" [9]. Thus three torque components are going to be discuses hereinafter .

2. Analysis

The motor construction is illustrated on Fig.1, and the driving circuit configuration is shown on Fig.2, where four MOSFET transistor bridge is illustrated. Taking into account the motor principle of operation, the armature winding is switched on for several instants with different durations during the operation period. This could be realized by applying PWM control strategy as it is shown on Fig.3. The reference modulation signal is chosen to be sinusoidal type with purpose to eliminate the highest order current harmonics .

2.1 : Armature Current

The armature current can be determined taking into account Fig.2, and the voltage balanced equation for both half periods as follows:

$$Vm = e(\alpha) + R\ i(\alpha) + L\ \frac{di}{d\alpha} + \Delta V$$

Where

$$Vm = +Vs \quad \text{for} \quad 0 \le \alpha \le \pi \qquad (1)$$

$$Vm = -Vs \quad \text{for} \quad \pi \le \alpha \le 2\pi$$

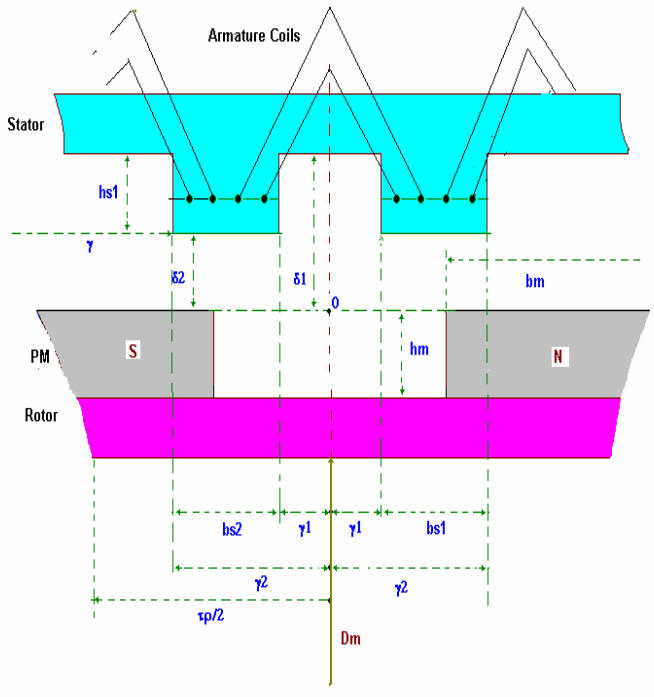

Fig.1. Partial section of the motor construction

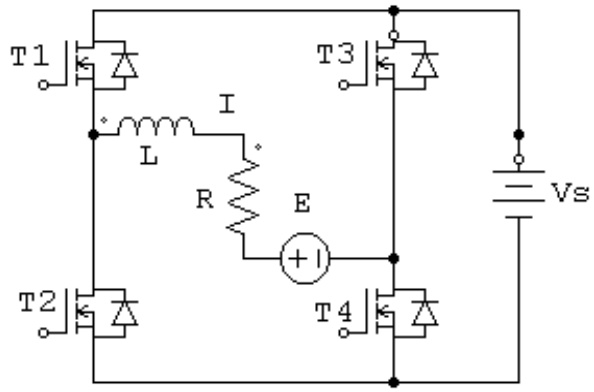

Fig.2. Electrical simplified circuit

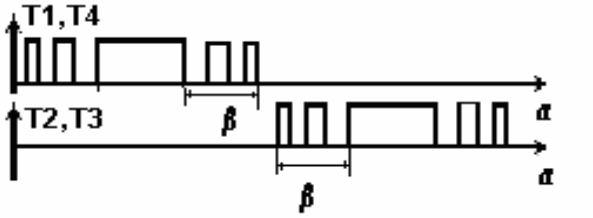

Fig.3. PWM signal wave form

The induced voltage in the armature winding depends on the flux density distribution in the air gap. This density can be determined analytically [9] by applying the field reflecting theory in Cartesian coordinate system as follows:

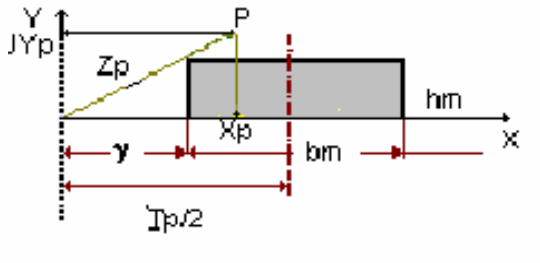

Fig. 4 Flux density in Cartesian coordinates

$$Bz(p) = Bx(p) - jBy(p)$$

Where

$$Bx(p) = \frac{\mu o\, A}{2\pi} \operatorname{Ln} \alpha x$$

$$By(p) = \frac{\mu o\, A}{2\pi} \alpha y$$

$$\alpha x = \frac{\sqrt{(Xp-\gamma-bm)^2+(Yp+hm)^2}}{\sqrt{(Xp-\gamma-bm)^2+Yp^2}} \cdot \frac{\sqrt{(Xp-\gamma)^2+Yp^2}}{\sqrt{(Xp-\gamma)^2+(Yp+hm)^2}}$$

$$\alpha y = \tan^{-1}\frac{Yp+hm}{Yp-\gamma} - \tan^{-1}\frac{Yp}{Yp-\gamma} + \tan^{-1}\frac{Yp}{Xp-\gamma-bm}$$

(2)

The Y-component distribution of magnetic flux density in the air gap and harmonic spectrum are illustrated on Fig.5.

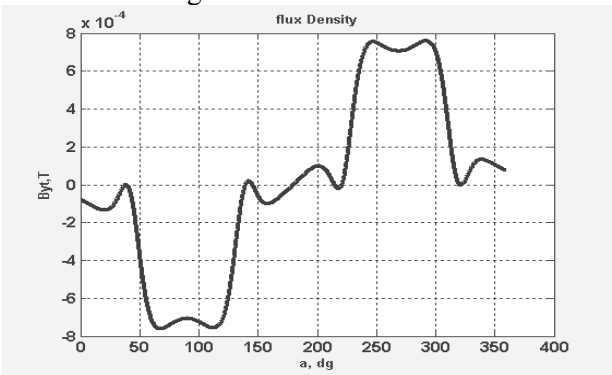

(a)

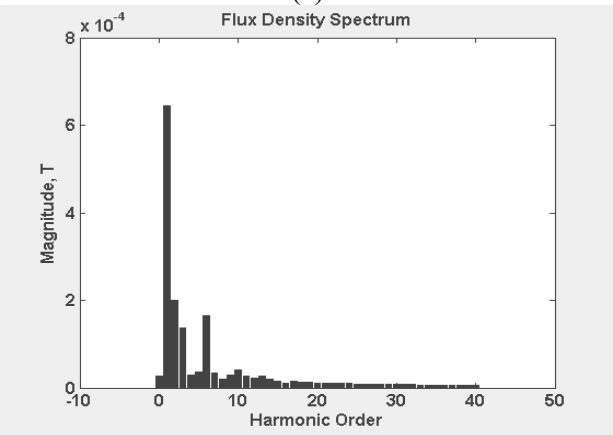

(b)

Fig.5: Magnetic field in the airgap: a) flux distribution, (b) harmonic spectrum .

Taking into account the flux harmonic spectrum, the induced voltage in the armature winding can be expressed as follows :

$$e(\alpha) = \sum_{odd} Em_\nu \sin(\nu\alpha)$$

Where

$$Em_\nu = Ce\,\omega Bm_\nu \qquad (3)$$

Since the distribution of the flux density in the airgap has a trapezoidal form, with neglected effect of 3rd harmonic of flux density, it can be assumed that the induced voltage has an approximately sinusoidal wave form.

The armature current can be determined taking into account eq.(1), and the method of implicit integration :

$$\int_{\alpha_1}^{\alpha_2} di = \frac{1}{\omega L}\int_{\alpha_1}^{\alpha_2}\left[Vs(\alpha) - e(\alpha) - R\ i(\alpha) - \Delta V\right]d\alpha \qquad (4)$$

By solving eq.(4), the phase current for certain speed and modulation index can be expressed :

$$i(\alpha_2) = \frac{1}{K(\alpha)}\left[V_{ph}(\alpha) - E_{ph}(\alpha) - V_R(\alpha)\right] \qquad (5)$$

where :

$$K(\alpha) = \left(1 + \frac{\Delta\alpha}{2} R\right)\omega L$$

$$V_{ph}(\alpha) = (Vm - \Delta V)\,\Delta\alpha$$

$$E_{ph}(\alpha) = \left[e(\alpha_1) + e(\alpha_2)\right]\frac{\Delta\alpha}{2}$$

$$e(\alpha_1) = Em \cdot \sin(\alpha_1)$$

$$e(\alpha_2) = Em \cdot \sin(\alpha_2)$$

$$V_R(\alpha) = R\ i(\alpha_1)\frac{\Delta\alpha}{2}$$

$$\Delta\alpha = \alpha_2 - \alpha_1$$

$$\text{At } \Delta\alpha \to 0 \Rightarrow d\alpha = \Delta\alpha$$

(6)

The phase voltage, back emf, and the phase current for certain speed and motor parameters are displayed on Fig.6.

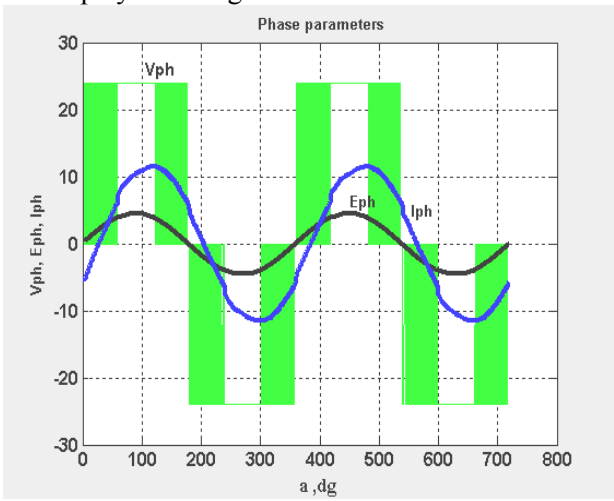

Fig.6. Phase Voltage, Emf, and Current at speed of 1000 rpm.

The current harmonic spectrum at the same speed obtained by applying FFT is displayed on Fig.7. In this figure it is shown that the armature current contains acceptable harmonic spectrum, which depends on the PWM modulation approach, motor speed and the control signal width .

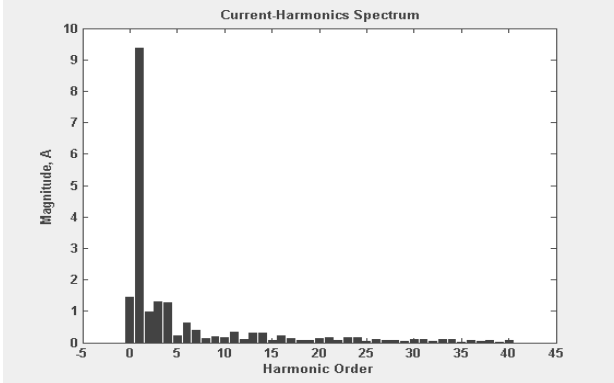

Fig.7. Current- harmonic spectrum.

As well mentioned above the quality of the armature current changes significantly by varying the speed as shown on Fig.8, where the harmonic effect being observable at high speed and neglected at low speed.

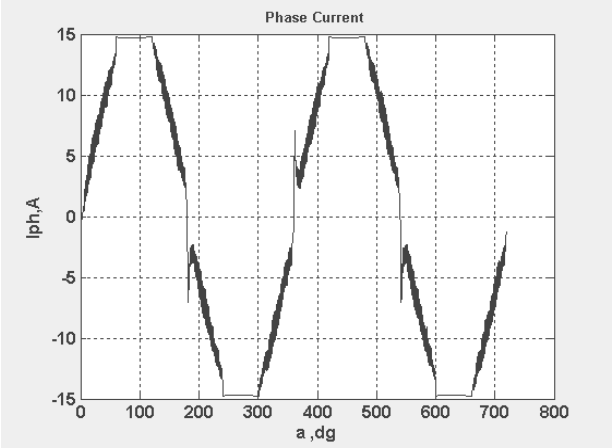

(a)

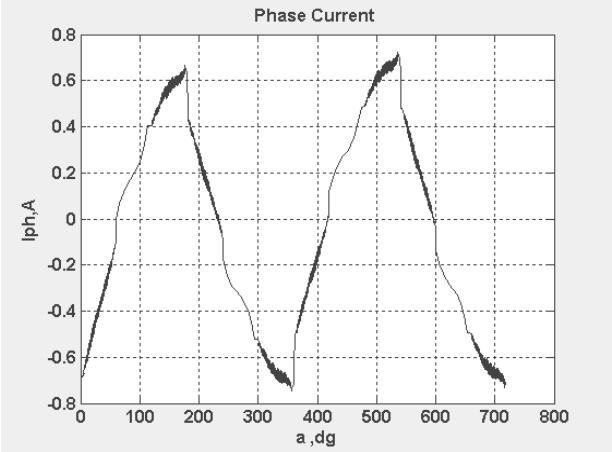

(b)

Fig.8. Armature current at speed of a) 100 rpm; b) 5000 rpm.

2.2 Electromagnetic Torque

The developed electromagnetic torque in the motor is divided into the following components:

2.2.1: ***Reluctance torque***: developed by the magnetic coenergy in the airgap and asymmetry in the stator interior periphery, therefore different permance in direct and quarter axis. This torque can be expressed as follows :

$$Tr(X) = -Dm\frac{\partial Wr_{(X,Y)}}{\partial X}$$

Where

$$Wr(X,Y) = \frac{Ls}{2\gamma o}\int_{x-\tau/2}^{x+\tau/2} B_y{}^2(x,y)dx$$

(7)

The instantaneous reluctance torque at given flux density and airgap geometry is shown on Fig.9.

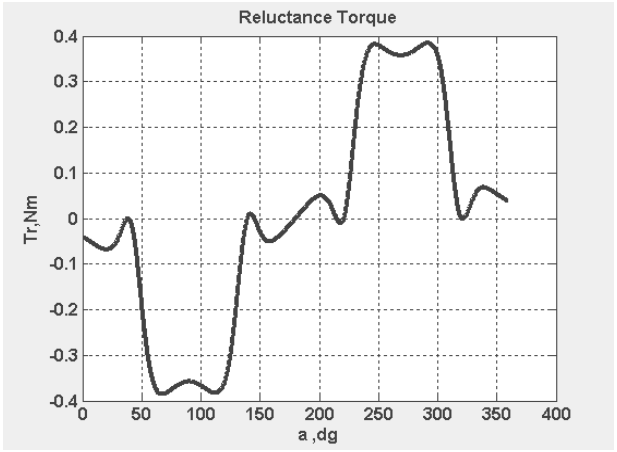

Fig.9. Motor reluctance torque.

2.2.2. ***Electromagnetic torque:*** developed by the interaction between the stator MMF and the magnetic field in the airgap. This torque can be expressed taking into account the current harmonic spectrum and stator net MMF as follows:

$$i_{(\omega t)} = Im\ 1\sum_{\nu} K_{\nu}\sin(\ \nu\omega\ t - \psi_{\nu})$$

(8)

The stator net MMF, as seen from a reference frame fixed to the stator [8-10], is

$$F(\alpha,\omega t) = \frac{2}{\pi} i(\omega t)\sum_{\nu} K_{w\gamma}\sin\gamma\alpha$$

(9)

The obtained electromagnetic torque due to the rotor magnetic flux and variable reluctance in the airgap is given by:

$$Tmr(\alpha) = \frac{d}{d\alpha} We(\alpha)$$

where

$$We(\alpha) = \tfrac{1}{2} G(\alpha)F^2(\alpha) + i(\omega t)N_{ph}\Phi m(\alpha)$$

$$\Phi m(\alpha) = Bm\,1.A_p\sum_{\beta} K_{\beta}\sin(\beta\alpha)$$

$$G(\alpha) = \frac{L(\alpha)}{(Nph\ K\omega)^2}$$

$$L(\alpha) = Lo + L_{2m}\sum_{\sigma=1,2} K_{\sigma}\cos(2\sigma\alpha)$$

(10)

Substituting (eq.8) and (eq.9) in (eq.10), writing the trigonometrically terms as sums and differences leads to the following expression for total instantaneous torque:

$$T_{mr}(\alpha) = T_{em}(\alpha) + T_{er}(\alpha) \qquad (11)$$

Where:

$$Tem(\alpha) = T_{MO}\sum_{\nu}\sum_{\gamma}\frac{K_\nu K_{w\gamma} K_\beta}{\gamma}\left(A_1 A_3 - A_2 A_4\right)$$

$$T_{MO} = D_s\, L_s\, N_{ph}\, Im_1\, B_{m1}$$

$$K_\nu = \frac{I_{m\nu}}{I_{m1}}; \quad K_\beta = \frac{B_{m\nu}}{B_{m1}};$$

$$A_1 = \cos(\gamma - \nu)\,\omega t; \qquad A_2 = \cos(\gamma + \nu)\,\omega t$$

$$A_3 = \cos\psi_\nu; \qquad A_4 = \sin\psi_\nu. \qquad (12)$$

$$Ter(\alpha) = \sum_{\nu}\sum_{\gamma}\sum_{\sigma}\left(B_1 + B_2 - B_3\right)$$

Where

$$B_1 = \frac{K^2_\nu}{\gamma} T_{MRO}\begin{pmatrix}\sin 2(\nu\omega t - \gamma\alpha) - \\ \sin 2(\nu\omega t + \gamma\alpha)\end{pmatrix}$$

$$B_2 = \frac{K^2_\nu}{\gamma} K_\sigma T_{MR2}\begin{pmatrix}\sin 2(\nu\omega t - \gamma\alpha) - \\ \sin 2(\nu\omega t + \gamma\alpha)\end{pmatrix}.\cos 2\sigma\alpha$$

$$B_3 = 2\sigma\frac{K^2_\nu}{\gamma^2} K_\sigma\, T_{MR2}\left(B_{31} + B_{32} - B_{33}\right).\sin 2\sigma\alpha \qquad (13)$$

$$B_{31} = \cos^2(\nu\omega t - \gamma\alpha)$$

$$B_{32} = \cos^2(\nu\omega t + \gamma\alpha)$$

$$B_{33} = 2(\cos 2\nu\omega t + \cos 2\gamma\alpha)$$

$$T_{MRO} = -\frac{L_O}{\pi^2} Im_1^2; \qquad T_{MR2} = -\frac{L_{2m}}{\pi^2} Im_1^2$$

$$K_\sigma = \frac{L_{m\sigma}}{L_{2m}}.$$

The first component of expression given in eq.(11) presents the electromagnetic torque, which depends on the rotor flux density. The second component presents the reluctance torque due to harmonic spectrum of the circuit inductance depending on the magnetic permance and air gap configuration.

The total electromagnetic torque with mathematical expression given in (eq.11) and torque harmonic spectrum are illustrated graphically on Fig.10 at speed of 1000 rpm .

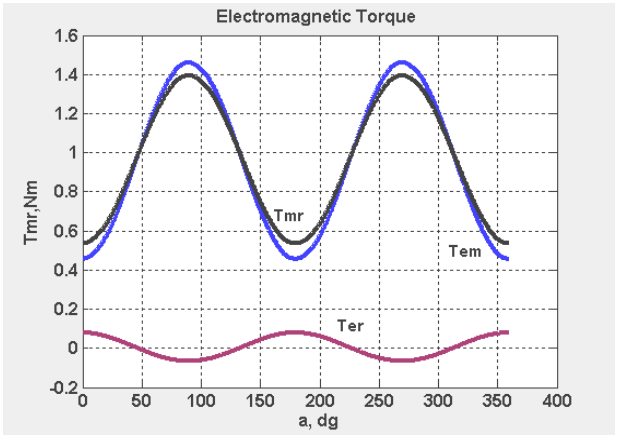

a) Electromagnetic torque

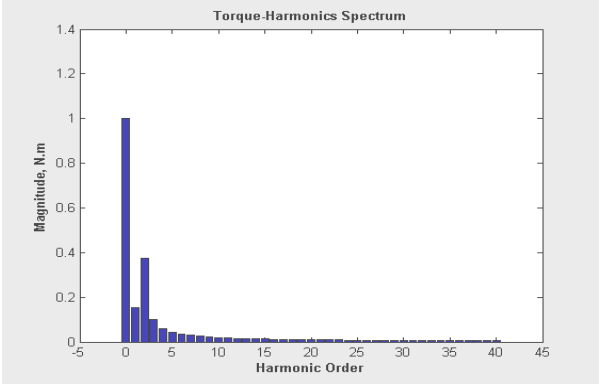

b) Torque harmonic spectrum

Fig.10. Electromagnetic Torque at speed of 1000rpm.

2.2.3: *The total motor torque*:

The total motor torque presents the sum of reluctance torque given in (eq.7) and electromagnetic torque given in (eq.11) as follows:

$$T_{tot}(\alpha) = T_{mr}(\alpha) + T_r(\alpha) \qquad (14)$$

Figure 11, illustrates the instantaneous total motor torque at various speeds 100 rpm, 1000 rpm & 5000 rpm , where it is clearly shown that there is no null torque points.

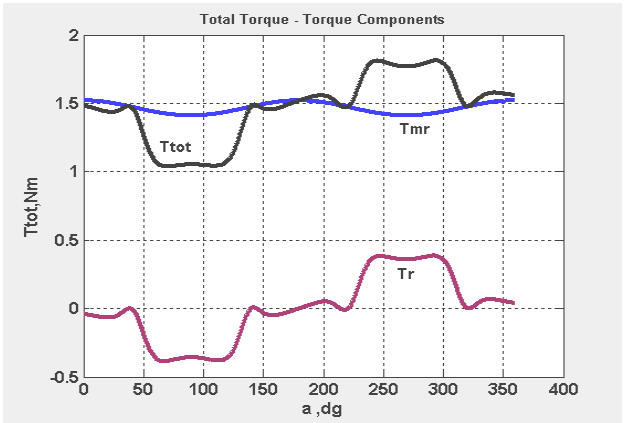

a) n=100 rpm

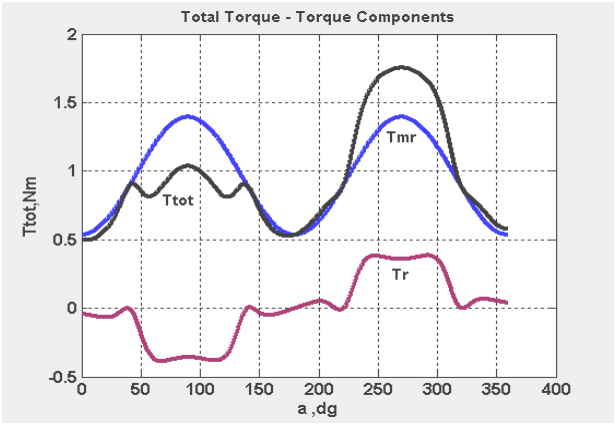

b) n= 1000 rpm

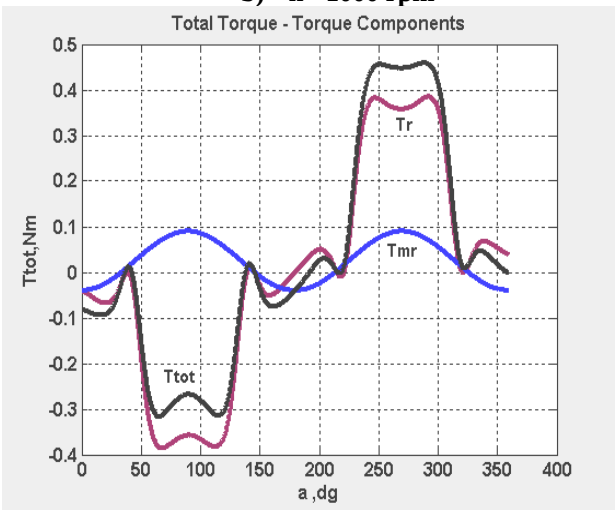

c) n=5000 rpm

Fig.11. Total motor torque at various speeds.

As well shown from these figures, the torque ripples increases significantly at high speed values and the dominant role lie on the reluctance torque.

3 . Simulation and Results

The motor overall quality can be verified by estimating the following parameters:

3.1 Torque-Current ratio : this parameter presents the ratio between the mean torque and the root-mean square current :

$$T_{CR} = \frac{T_{AV}}{I_{TRMS}}; \qquad I_{TRMS} = \sqrt{\sum_{v=1,3,5}^{\infty} I_{RMSv}^2} \qquad (15)$$

3.2 Torque ripple factor: this parameter presents the ratio between torque ripples and motor mean torque :

$$T_{RR} = \frac{T_T}{T_{AV}};$$

$$T_T = \sqrt{\frac{1}{T}\int_0^{2\pi} (T_{tot} - T_{AV})^2 d\alpha} \qquad (16)$$

3.3: Current harmonic factor: this parameter presents the ratio between the total rms current and the fundamental value :

$$H_{FI} = \sqrt{\left(\frac{I_{TRMS}}{I_{RMS}}\right)^2 - 1} \qquad (17)$$

The motor rms current, torque-current ratio, torque-ripples factor, and current harmonic factor varies by regulating the width of the pulse control signal β and motor speed. Such relations are illustrated on Fig.12 -Fig.15, for β1=60°, β2=30°, & β3=20°.

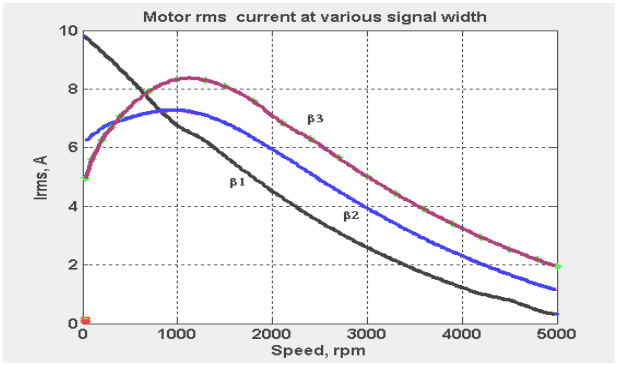

Fig.12: The rms current vs motor speed at different control signal width β .

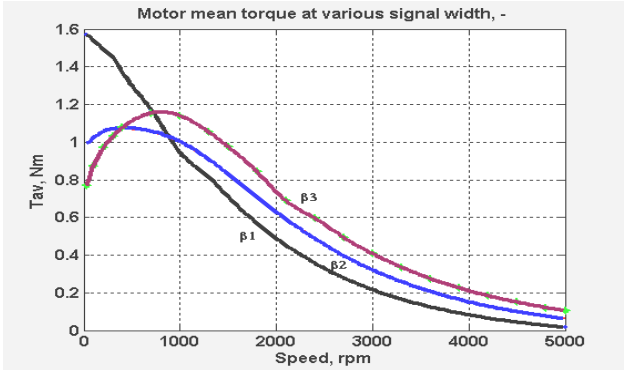

Fig.13: The motor mean torque at various motor speed & control signal width β.

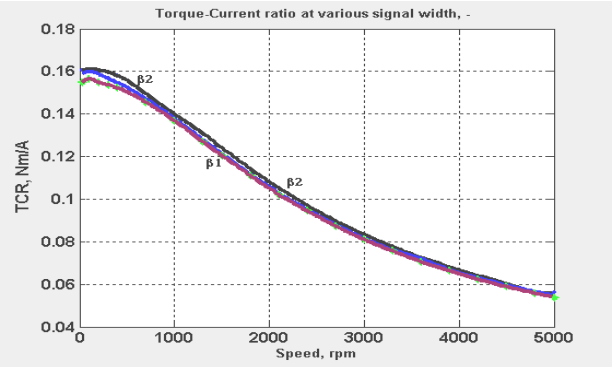

Fig.14: The torque-current ratio at various motor speed & control signal width β.

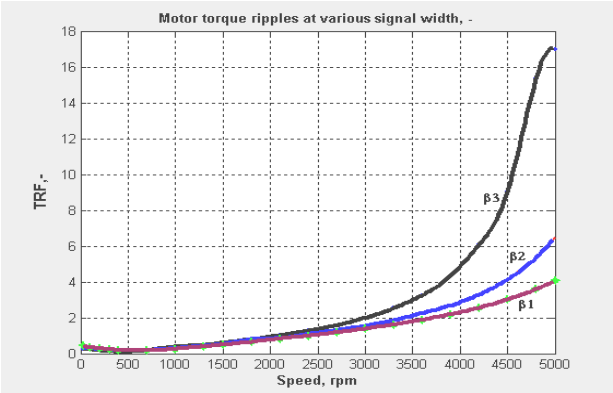

Fig.15: The torque ripples at various motor speed & control signal width β .

As the control signal width varies in wide range, the motor current and torque can also vary in the same manner. Fig.16, Fig.17 and Fig.18 illustrates the change of current and torque by varying the control signal width at speeds of n1=500, n2=1500, n3=3000, n4=4500, and n5=5000 rpm.

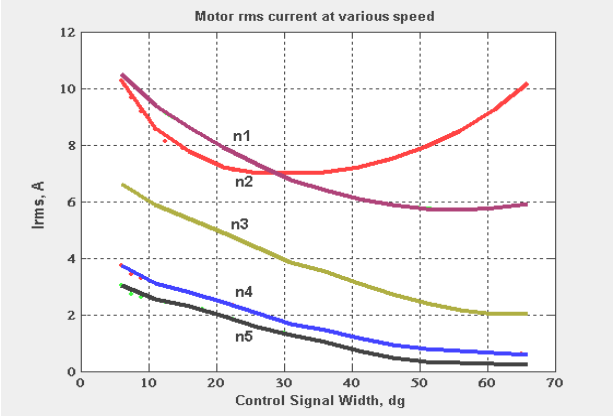

Fig.16: The motor rms current at various control signal width β and speed.

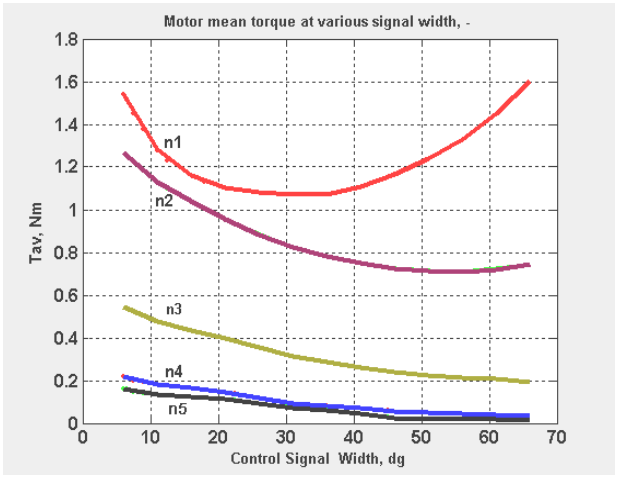

Fig.17: The motor mean torque at various control signal width β and speed .

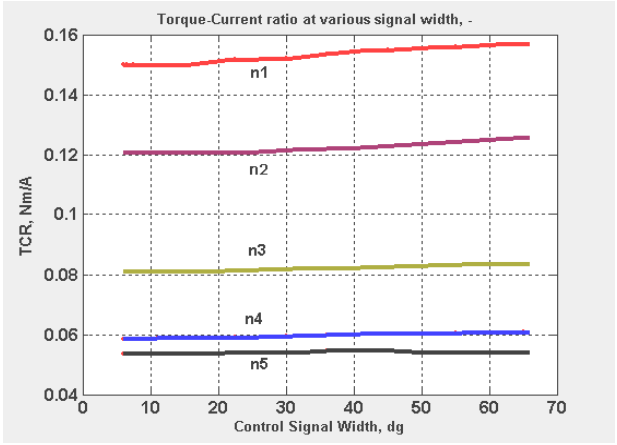

Fig.18: The motor torque –current ratio at various control signal width β and speed.

4. Conclusion

1- The applied design of single phase/ single coil brushless DC motor with PWM strategy produced electromagnetic torque has self-starting and relatively reduced fluctuation. This is due to the interior stator configuration, and the applied PWM strategy .

2- The asymmetrical configuration of the interior stator periphery produced an additional reluctance torque that depends on the flux distribution in the airgap.

3- While the duration of sub-control signals (train of pulses) decreases, the pulse width β increases, the current and torque behaviors being similar to square control signal, where additional harmonics should be injected in the system.

4- By introducing the PWM control strategy with variable signal width **β,** the motor mean torque can vary in wide range and the torque ripples can

respond to the variation**,** therefore maximized the mean torque and minimized the torque ripples that achieved at certain value of β. Once torque ripples decreases, the motor stability enhances, the dissipated power reduces and motor utility increases .

5- The motor torque-current ratio remains approximately unaffected by changing β, while this value decreases by raising the motor speed.

5. List of Symbols

Vs	The supply voltage
Vm	The voltage across the armature terminals
$e(\alpha)$	The instantaneous value of the induced voltage
$i(\alpha)$	The instantaneous value of the phase current
R	Armature resistance
L	Armature inductance
ΔV	Voltage drop across the switches T1,T4 , & T2, T3
Bx(p)	The X-component of Flux density at point p
By(p)	The Y-component of Flux density at point p
Bz(p)	The Z-component of Flux density at point p
μo	The magnetic permeability at vacuum
$\alpha 1$, $\alpha 2$,	The sub pulse duration of the train PWM pulses
A	The magnetic intensity
hm	Magnetic depth
bm	Magnetic width
$Em\nu$	The magnitude of ν-ti harmonic of induced e.m.f.
Ce	Machine constant
ω	Angular frequency
$Bm\nu$	The magnitude of ν-ti harmonic of flux density
Tr	Reluctance component of the developed torque.
Wr	The magnetic coenergy
Dm	Rotor diameter including the magnetic depth.
Ls	Stator active length
p	Number of magnetic poles
Im1	Fundamental current harmonic
$K\nu$	The ratio of ν-ti current harmonic to the fundamental value
ν	ν-ti order of the time harmonic
$\psi\nu$	The phase shift of the ν-ti current harmonic
$F(\alpha,\omega t)$	The armature mmf with space-time distribution
$Kw\nu$	The winding factor of γ-ma space harmonic
γ	γ-ma order of the space harmonic
Tem	The electromagnetic component of the torque
Ter	The reluctance component of the torque
Tmr	The total electromagnetic torque
We	The magnetic energy produced by the permanent magnet, and the magnetic permance
Φm	Magnetic flux in the airgap
$K\beta$	The ratio of β-ta flux density harmonic to the fundamental value
Lo	The constant value of the circuit inductance
L2m	The magnitude of the second harmonic of the circuit inductance
σ	Harmonic order of circuit permance, and inductance
G	Magnetic permance in the airgap
$K\sigma$	The ratio of σ-ma harmonic of the circuit inductance to the second harmonic
Ttot	The overall developed torque in the motor.
TCR	Torque –current ratio
TAV	Mean value of total electromagnetic torque
ITRMS	Total root mean square of the armature current
$IRMS\nu$	Root mean square of the highest current harmonic order
TRR	Torque ripple ratio
HFI	Current harmonic factor

6. References

[1] Alexander Kusko and Syed M. Peeran, " Brushless DC motor using usymmetrical Field magnetization " , in proc. IA Vol.23, No.2, march/april 1987, p.319.

[2] Bolton H. R. and Ashen R.A. , " influence of motor design and feed-current waveform on torque ripple in brushless dc motor", IEE proc. Vol.131, pt.B, No.3, may/1984, pp.82 –90.

[3] Sameer H. Khader, " Implementation Of An Accurate Mathematical Method For Modeling Electromagnetic Processes of Brushless DC Motor", MESM'2001, Amman 2-3 /Sept. Jordan, pp.31-38.

[4] Miller, T. J. E., " Switched Reluctance Motors and their Control, Oxford /UK, Magna Phys. Publication and Clarendon, press 1993.

[5] Faiz, J. and Finch J.W.," Aspects of design optimization for Switched Reluctance Motors", IEEE trans. On energy conversion 8, 1993, No.4, pp.704 .

[6] Torrey D.A., Niu X.M. and Unkauf, E.J., " Analytical Modelling of Variable-Reluctance machine Mgnetization characteristics. IEEE proc.B-142/ 1995, No.1, pp.14-22 .

[7] Cathey J. J. and Krimm T. W., " A Theoretical Study of Reduction of Torque Pulsations in Low-Speed Self-Synchronous MotorDrives fed through a Cycloconverter Link.", Electric Machines and Power systems, No.13, 229-243, 1987, Hemisphere Publ. Corp.

[8] Krimm T.W, " harmonic Control to reduce torque Pulsations in brushless DC Motor Drives", MSEE Thesis, University of Kentucky , 1984.

[9] Abdel Kareem Daud, " Single phase Brushless dc motor with air-winding', Ph.D thesis, TU-Berlin, Germany 1990.

[10] Stephen Chapman, " Electric machines Fundamentals", 3rd ed. 1998, McGraw-Hill International Edition.